CHAPTER IV

METHANOL SYNTHESIS WITH SLURRY CIRCULATION

4.1 Introduction

The operations of liquid phase methanol process at Air Products' (1987) LaPorte pilot plant have significantly advanced development of the technology for producing methanol from coal conversion gases. Although a great deal of progress was made in demonstrating the liquid-entrained mode of operation with circulation of slurry, the RUN E-2 series also revealed that more research must be conducted if the slurry bubble column reactor is to achieve the performance of the bench-scale reactors at high slurry loadings. The hydrodynamics of the reactor deserves further study to understand the cause of the axial solid density profile observed in the bottom section of the reactor while operating with high slurry concentrations. Slurry properties such as viscosity, which may affect the reactor performance and hydrodynamics, should be determined at operating conditions.

Viking System Internationals (1993) had developed an one-dimensional, steady state model to design slurry bubble column reactors. Their model can not predict the reactor hydrodynamics. In this chapter, IIT's hydrodynamic model has been modified with methanol reaction and used to simulate slurry bubble column reactor's dynamic behaviors (WU and Gidaspow 1994).

4.2 Reaction, Kinetics and Mass transfer

4.2.1 Reaction and Kinetics. In the synthesis of methanol from syn-gas, a coal conversion gas, the following chemical reactions primarily discussed:

$$CO+2H_2=CH_3OH \qquad (a)$$

$$CO_2+H_2=CO+H_2O \qquad (b)$$

$$CO_2+3H_2=CH_3OH+H_2O \qquad (c)$$

Several researchers had investigated the kinetic rate for methanol synthesis. There two kinds of models proposed, power law rate expressions and mechanistic models.

A mechanistic model was developed by Lee (1990):

$$r_{MeOH} = A\exp\left(-\frac{E}{RT}\right)\left(C_{H_2} - C_{H_{2,eq}}\right)$$

$$A = 3380cm^3/kg\cdot s \qquad E = 18{,}800kcal/kmol$$

This model does not account for partial pressure of carbon monoxide,

Wedel et al. (1982) developed a power law rate expression based on a review of various literature models:

$$r=\varepsilon_s\rho_s\left\{1.98\times10^7\exp(-56343/RT)P_{H_2}^{0.4}P_{CO}^{0.18}-2.15\times10^{10}\exp(-85930/RT)P_{CH_3OH}^{0.13}\right\}$$

This model is used in this simulation and a mechanistic model, provided by Air Products (1992) kinetics research, has been used in the simulation of chapter 5.

4.2.2 Mass Transfer Between Gas and Liquid Phase. The mass transfer rate can be expressed as:

$$R_j=\varepsilon_l K_{jl} a(C_j^{g-l}-C_j^l)$$

Where C_j^l is bulk concentration of species j and $C_j^{g\text{-}l}$ is concentration of species j at gas-liquid interface which can be defined by Henry law:

$$C_{jl}^{g-l}=\frac{f_j}{H_j}$$

Graff et al. (1988) measured solubilities of syn-gas in the temperature of 210 to 260°C in a high molecular weight solvent. Their temperature depended Henry constants could be used with LaPorte's operating conditions.

$$H_{CO}=0.175\exp(638/RT)$$
$$H_{CO_2}=0.402\exp(-6947/RT)$$
$$H_{H_2}=0.0782\exp(4875/RT)$$
$$H_{CH_3OH}=1.49\exp(-17235/RT)$$

4.3 Species Balance

Gas Phase:

$$\frac{\partial}{\partial t}(\varepsilon_g\rho_g y_g^j)+\nabla\cdot(\varepsilon_g\rho_g y_g^j v_g)=\frac{\alpha^j\varepsilon_s\rho_s M^j r}{3.6\times10^6}-\varepsilon_\ell M^j R_j$$

Liquid Phases:

$$\frac{\partial}{\partial t}(\varepsilon_k\rho_k y_k^j)+\nabla\cdot(\varepsilon_k\rho_k y_k^j v_k)=\varepsilon_\ell M^j R_j$$

$$\sum_j^N y_k^j=1 \qquad k=g,\ell$$

j=	CO	CO_2	H_2	CH_4	CH_3OH	wax
α^j=	−1	0	−2	0	1	0

The phase changes, consisting of mass transfer of species between gas and liquid, will be used in the hydrodynamic models described in section 4.4:

$$\dot{m}_\ell=\varepsilon_\ell\sum_j^N M^j R_j \qquad \dot{m}_g=-\dot{m}_\ell \qquad \dot{m}_s=0$$

4.4 Mathematical Models (Empirical)

No energy equation is needed in this simulation because of isothermal assumption. The empirical models for solid pressure and viscosity are used. The kinetic theory approach will be used in other computations depicted in chapter 5 and 6.

4.4.1 Continuity Equations

Gas Phase:

$$\frac{\partial}{\partial t}(\varepsilon_g \rho_g)+\nabla\cdot(\varepsilon_g \rho_g \mathbf{v}_g)=\dot{m}_g$$

Liquid and Solid Phases: ($k=\ell,s$)

$$\frac{\partial}{\partial t}(\varepsilon_k \rho_k)+\nabla\cdot(\varepsilon_k \rho_k \mathbf{v}_k)=\dot{m}_k$$

4.4.2 Momentum Equations

Gas Phase:

$$\frac{\partial}{\partial t}(\varepsilon_g \rho_g \mathbf{v}_g)+\nabla\cdot(\varepsilon_g \rho_g \mathbf{v}_g \mathbf{v}_g)=\varepsilon_g \rho_g \mathbf{F}_g+\sum_{m=\ell,s}\beta_{gm}(\mathbf{v}_m-\mathbf{v}_g)+\nabla\cdot[\tau_g]+\dot{m}_g \mathbf{v}_g$$

Liquid and Solid Phases: ($k=\ell,s$)

$$\frac{\partial}{\partial t}(\varepsilon_k \rho_k \mathbf{v}_k)+\nabla\cdot(\varepsilon_k \rho_k \mathbf{v}_k \mathbf{v}_k)=\varepsilon_k \rho_k \mathbf{F}_k+\sum_{m=g,\ell,s}\beta_{km}(\mathbf{v}_m-\mathbf{v}_k)+\nabla\cdot[\tau_k]+\dot{m}_k \mathbf{v}_k$$

4.4.3 Constitutive Equations

$$\varepsilon_g+\varepsilon_\ell+\varepsilon_s=1$$

Equation of State:

$$\rho_g=\frac{\overline{M}_g P_g}{zRT_g}$$

Drag Coefficients: ($k=\ell,s$) (Based on Ergun Equation)

$$\beta_{gk}=\beta_{kg}=150\frac{(1-\varepsilon_g)\varepsilon_k \mu_g}{(\varepsilon_g d_k \psi_k)^2}+1.75\frac{\rho_g \varepsilon_k |\mathbf{v}_g-\mathbf{v}_k|}{\varepsilon_g d_k \psi_k} \qquad \varepsilon_g>0.8$$

$$\beta_{gk}=\beta_{kg}=\frac{3}{4}C_D\frac{\rho_g \varepsilon_k |\mathbf{v}_g-\mathbf{v}_k|}{d_k \psi_k}\varepsilon_g^{-2.65} \qquad \varepsilon_g<0.8$$

$$\beta_{\ell s}=\beta_{s\ell}=\frac{3}{2}(1+e)\frac{\rho_s\rho_\ell\varepsilon_s\varepsilon_s|v_\ell-v_s|}{\rho_s d_s^3+\rho_\ell d_\ell^3}(d_s+d_\ell)^2$$

where

$$C_D=\frac{24}{Re_k}(1+0.15Re_k^{0.687})$$

$$Re_k=\frac{\rho_g\varepsilon_g|v_g-v_k|d_k\psi_k}{\mu_g} \qquad Re_k=1000 \quad \text{if} \quad Re_k>1000$$

External Forces Acting on Each Phase:

$$F_g=\frac{g}{\varepsilon_g}$$

$$F_k=\frac{g}{\varepsilon_g}\left(1-\frac{1}{\rho_k}\sum_{m=g,\ell,s}\varepsilon_m\rho_m\right) \qquad k=\ell,s$$

Shear Stresses:

$$[\tau_g]=\left\{-P_g-\frac{2}{3}\mu_g\varepsilon_g\nabla\cdot v_g\right\}[I]+\mu_g\varepsilon_g\left[\nabla v_g+(\nabla v_g)^T\right]$$

$$[\tau_k]=\left\{-P_k+\tau_{ck}+(\xi_k-\frac{2}{3}\mu_k)\nabla\cdot v_k\right\}[I]+\mu_k\left[\nabla v_k+(\nabla v_k)^T\right] \qquad k=\ell,s$$

Cohesive Force: $\tau_{ck}=10^{10.6\varepsilon_k+5.5}$ $\qquad k=\ell,s$

Empirical Solids Pressure and Viscosity: ($k=\ell,s$)

$$\mu_k=5\varepsilon_k \qquad \xi_k=0$$

$$\nabla P_k=G(\varepsilon_k)\nabla\varepsilon_k \qquad G(\varepsilon_k)=10^{8.76\varepsilon_k-0.27}$$

4.5 Operating Conditions

The operating conditions are same as those of LaPorte's RUN E-2-B (Air Products 1987).

The operating conditions are summarized as following.

Diameter of the reactor	59 cm
Height of the reactor	600 cm
Superficial gas velocity	11.9 cm/s
Superficial liquid velocity	4.9 cm/s
Superficial solid velocity	4.9 cm/s
Temperature	250 ^{o}C
Pressure	6,310 kPa
Catalyst diameter	50 μm
Catalyst concentration	46.06%(wt)
Liquid	wax
Density of liquid	0.70025 g/cm^3
Number of cells in the grid	18x33
Time interval	10^{-4} sec.

4.6 Numerical Considerations

4.6.1 Initial Conditions. The initial gas, liquid and solid volume fractions and velocities are assumed to be uniform over the whole bed. A constant pressure, 6.31 MPa, is kept at the top of the bed and isothermal is assumed in these simulation runs. The initial conditions are summerized as followings:

gas	liquid	solid
$\varepsilon_g=0.3800$	$\varepsilon_\ell=0.4805$	$\varepsilon_s=0.1395$
$u_g=0$	$u_\ell=0$	$u_s=0$
$v_g=31.3cm/s$	$v_\ell=7.9cm/s$	$v_s=7.9cm/s$

Syn-gas composition:

		CO	CO_2	H_2	CH_4	CH_3OH
%mol		19.33	4.05	59.34	17.05	0.24
y_g^j	%wt	48.39	15.93	10.61	24.38	0.69

4.6.2 Boundary Conditions. The inflow conditions, including gas, liquid and solid velocities and volume fractions, and the top pressure are prescribed. Assumption of non-slip at the walls is made for both gas and liquid phases. The boundary conditions around the computing mesh, shown as Figure 4.1, are summerized as following.

	gas	liquid	solid
bottom	$\varepsilon_g=0.3800$	$\varepsilon_\ell=0.4805$	$\varepsilon_s=0.1395$
	$v_g=31.3cm/s$	$v_\ell=7.9cm/s$	$v_s=7.9cm/s$
	$u_g=0$	$u_\ell=0$	$u_s=0$
	$y_g^j=y_g^{j0}$	$y_\ell^j=0$	$y_s^j=0$
left/right	$v_g=0$	$v_\ell=0$	$v_s=0$
	$u_g=0$	$u_\ell=0$	$u_s=0$
top	$\frac{\partial \varepsilon_g}{\partial y}=0$	$\frac{\partial \varepsilon_\ell}{\partial y}=0$	$\frac{\partial \varepsilon_s}{\partial y}=0$
	$\frac{\partial v_g}{\partial y}=0$	$\frac{\partial v_\ell}{\partial y}=0$	$\frac{\partial v_s}{\partial y}=0$
	$u_g=0$	$u_\ell=0$	$u_s=0$
	$\frac{\partial y_g^j}{\partial y}=0$	$\frac{\partial y_\ell^j}{\partial y}=0$	$\frac{\partial y_s^j}{\partial y}=0$

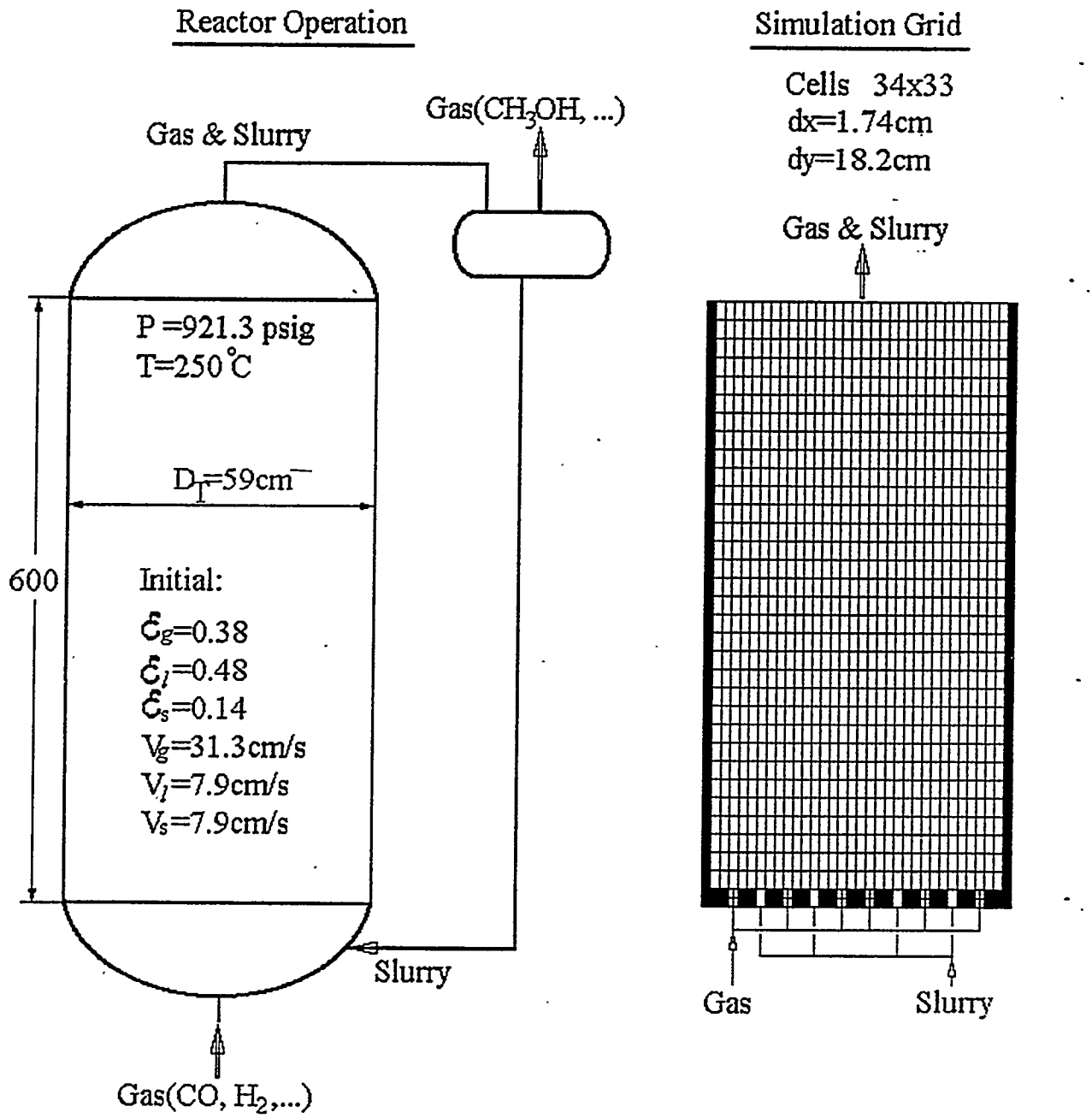

Figure 4.1 Reactor Operation with Slurry Circulation and Simulation Grid

4.6.3 Computation. Finite difference method is used to solve these partial differential equations simultaneously and the values of following variables at each time step and cell position can be obtained.

$$\varepsilon_g, \varepsilon_\ell, \varepsilon_s, v_g, v_\ell, v_s, P_g, y_g^j, y_\ell^j, y_s^j$$
$$j = CO, CO_2, H_2, CH_4, CH_3OH, wax$$

4.7 Computational Results and Discussions

The computing run was performed on a HP735 Workstation and the simulation time is 40 seconds. All data are taken by time and cross section area average over the period of last ten seconds.

Table 4.1 lists the material balance of the simulations and Table 4.2 lists the comparison of simulation and LaPorte's RUN E-2-B. They show very close CO conversions. The computed rate of methanol production is a little higher than that of RUN E-2-B since the kinetic model does not reflect exactly reactor performance.

Table 4.1 Material Balance: ($CO:H_2=1:3$)

	Inlet		Outlet	
	% mol	kgmol/hr	% mol	kgmol/hr
CO	19.33	33.7	16.40	25.9
CO_2	4.05	7.0	4.40	7.0
H_2	59.34	103.3	55.50	87.5
CH_3OH	0.24	0.4	5.00	7.9
CH_4	17.05	29.5	18.70	29.5
$\overline{M}$ (kg/kgmol)	11.18		12.23	
Flowrate (kgmol/hr)		173.9		157.8
Flowrate (kg/hr)		1945		1930

Table 4.2 Comparison of Simulation and Air Products' (1987) RUN E-2-B:

	CO conv. (%)	Slurry conc. (%wt)	Total catalyst (kgmole/hr)	CH_3OH (gmol/hr/kg)	Net CH_3OH (TPD)
Simulation	22.3	46.4	7.9	10.88	6.07
RUN E-2-B	21.3	48.9	7.3	9.9	5.60

Figure 4.2 shows a comparison of computed and measured catalyst concentrations for LaPorte reactor. At zero time the concentration was uniform. After 20 seconds the density at the bottom of the reactor increased substantially. The computed and experimental profiles match reasonably well.

Figure 4.3 shows the computed axial profiles for gas, liquid and solid three phases; Figure 4.4 shows the methanol concentration profiles in both gas and liquid phases.

Figure 4.5a--c show a series of catalyst concentration distribution as a function of time. After startup, catalyst-free voiage are forming and propagating with time elasting. These voidages significantly reduce the reactor performance.

Figure 4.6a--c show a series of methanol concentration propagation as a function of time. The concentration is getting dense until a final steady state.

In summary, the computed catalyst concentration profile and the rate of methanol production agree well with the measurements obtained at LaPorte pilot plant. The dynamic simulation results such as the time series catalyst distributions are very helpful for the understanding of the reactor hydrodynamic behavior.

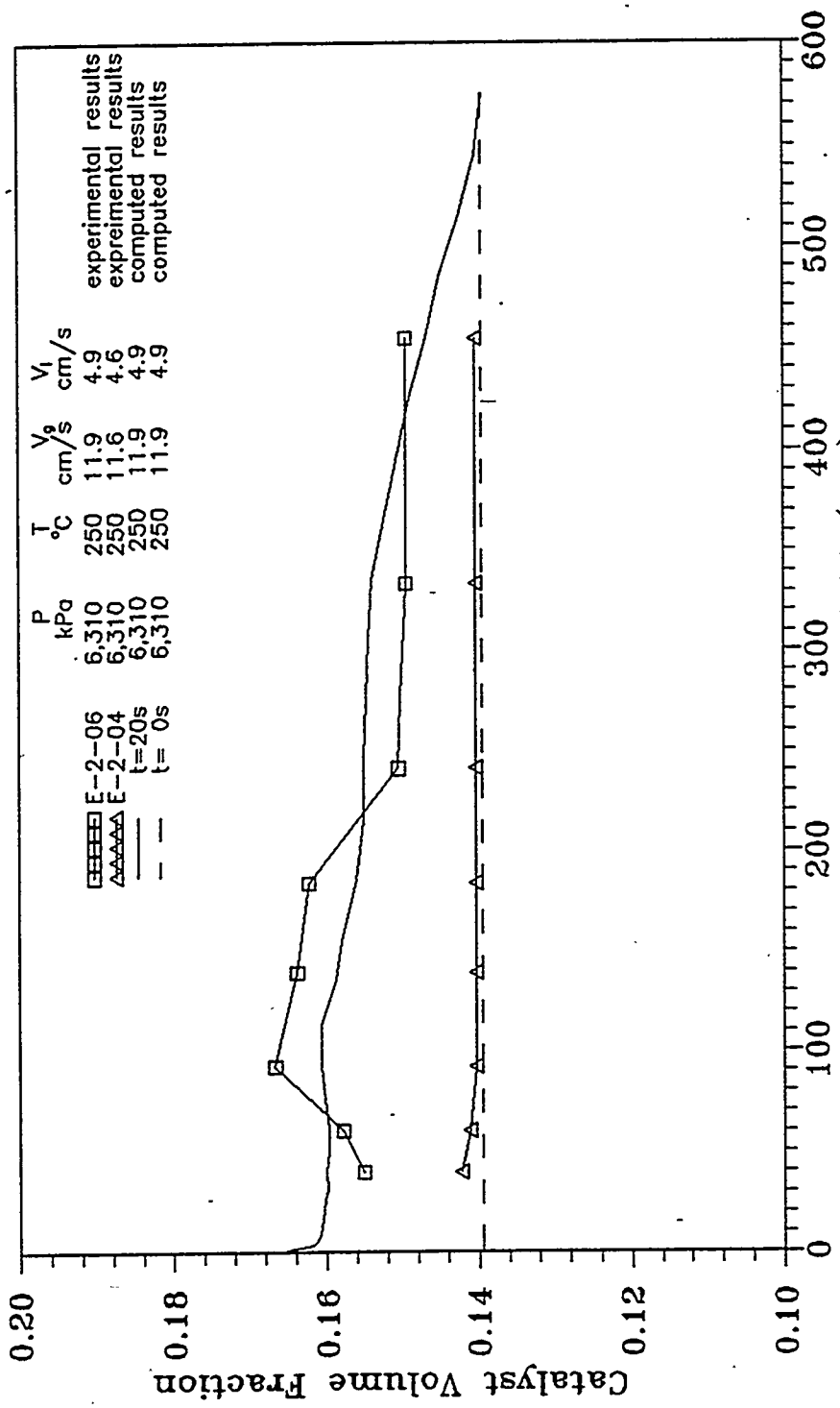

Figure 4.2 Computed and Experimental Axial Catalyst Volume Fraction Profiles

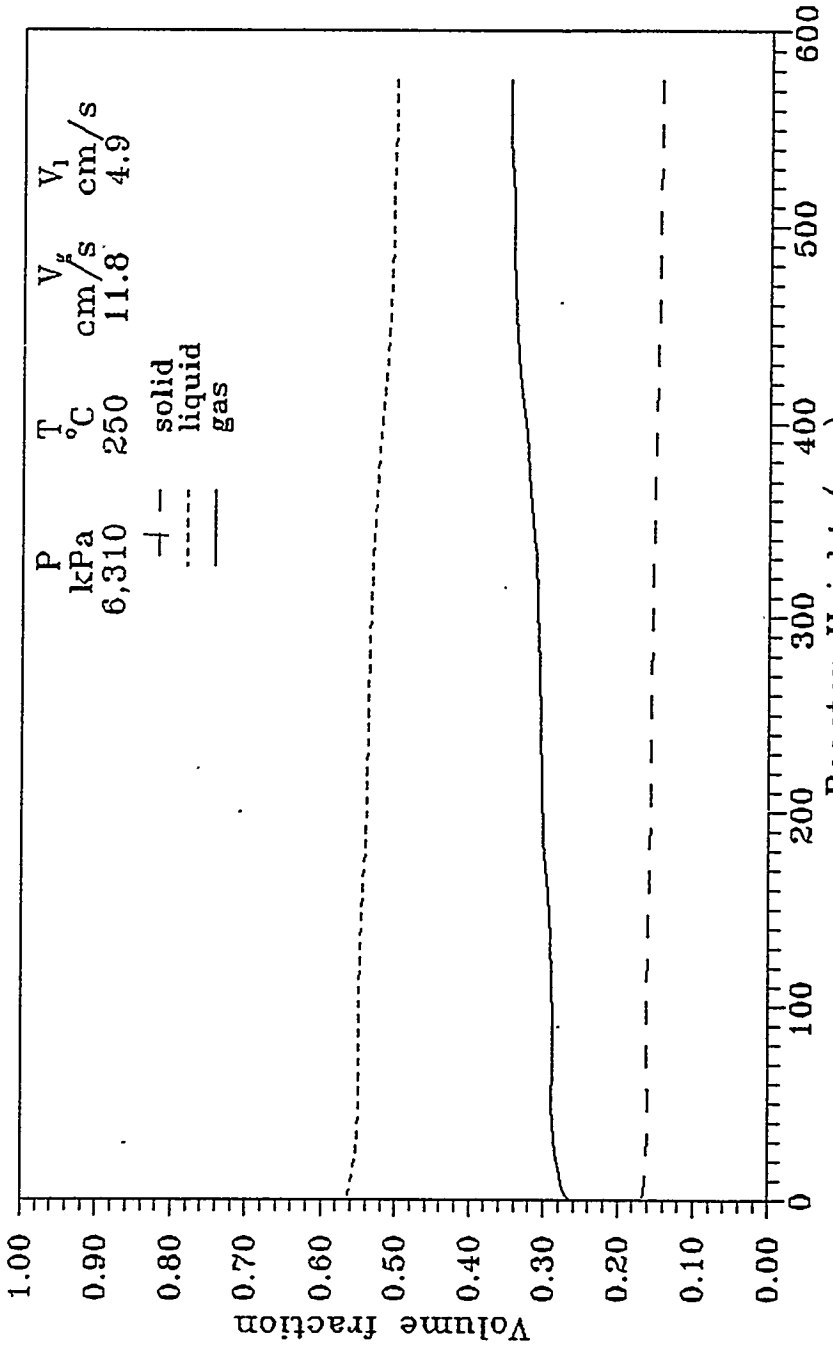

Figure 4.3 Computed Gas, Liquid and Solid Axial Volume Fraction Profiles

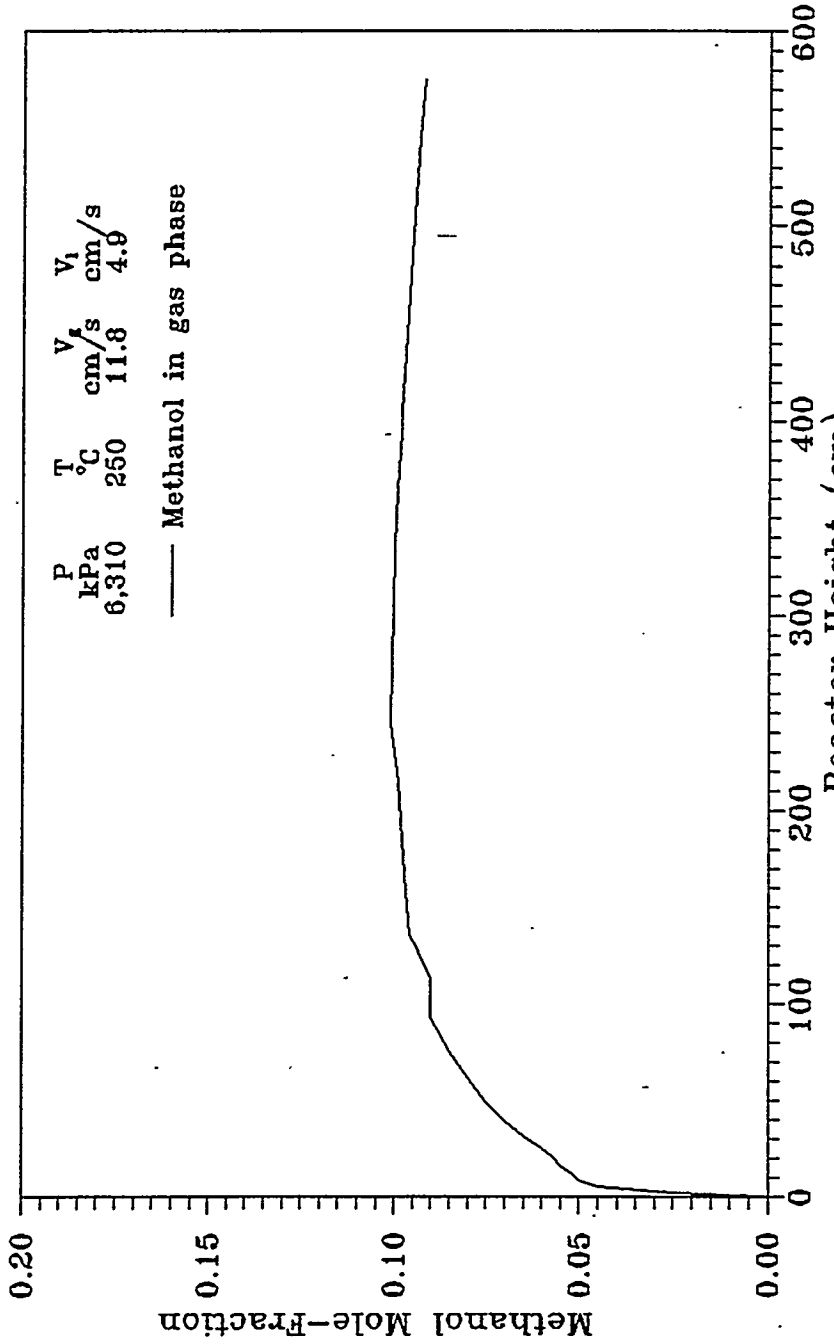

Figure 4.4 Computed Axial Methanol Concentration Profile

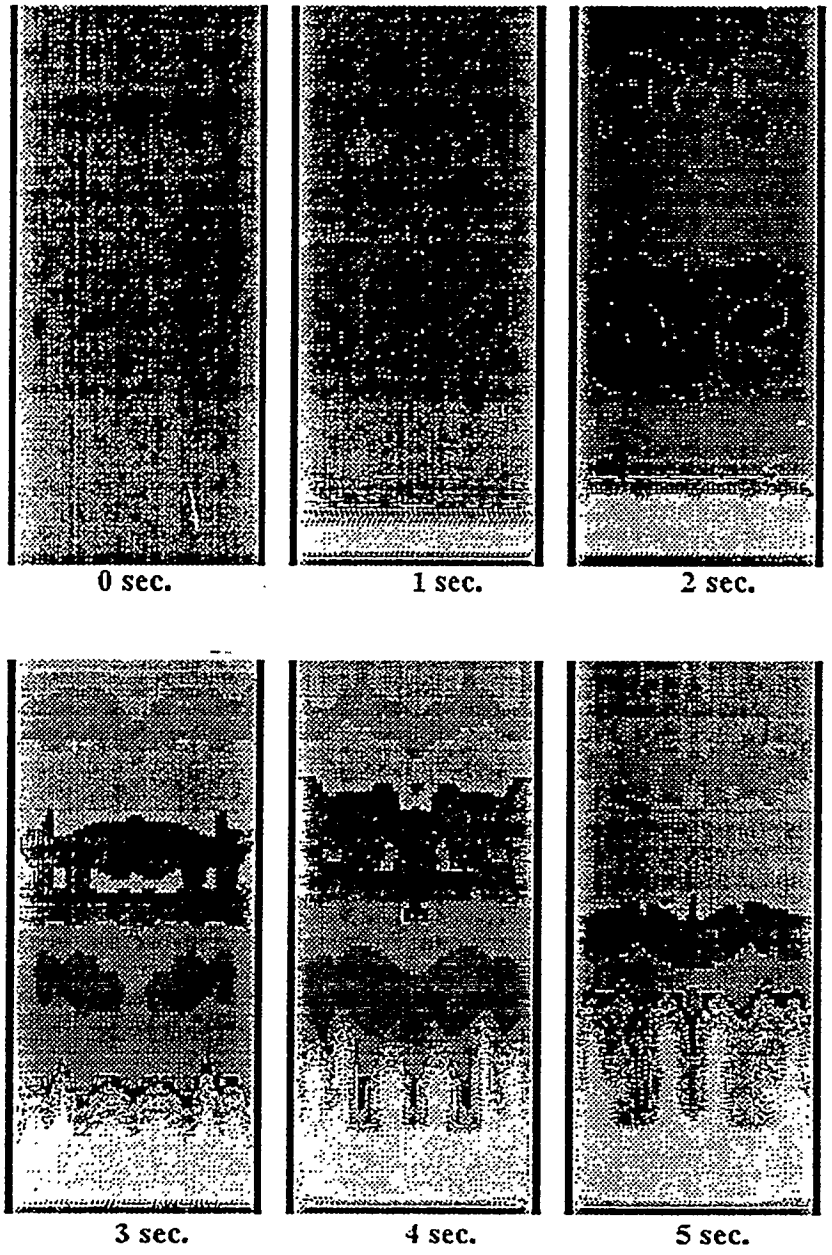

Figure 4.5a The Catalyst Concentration Profiles as a Function of Time

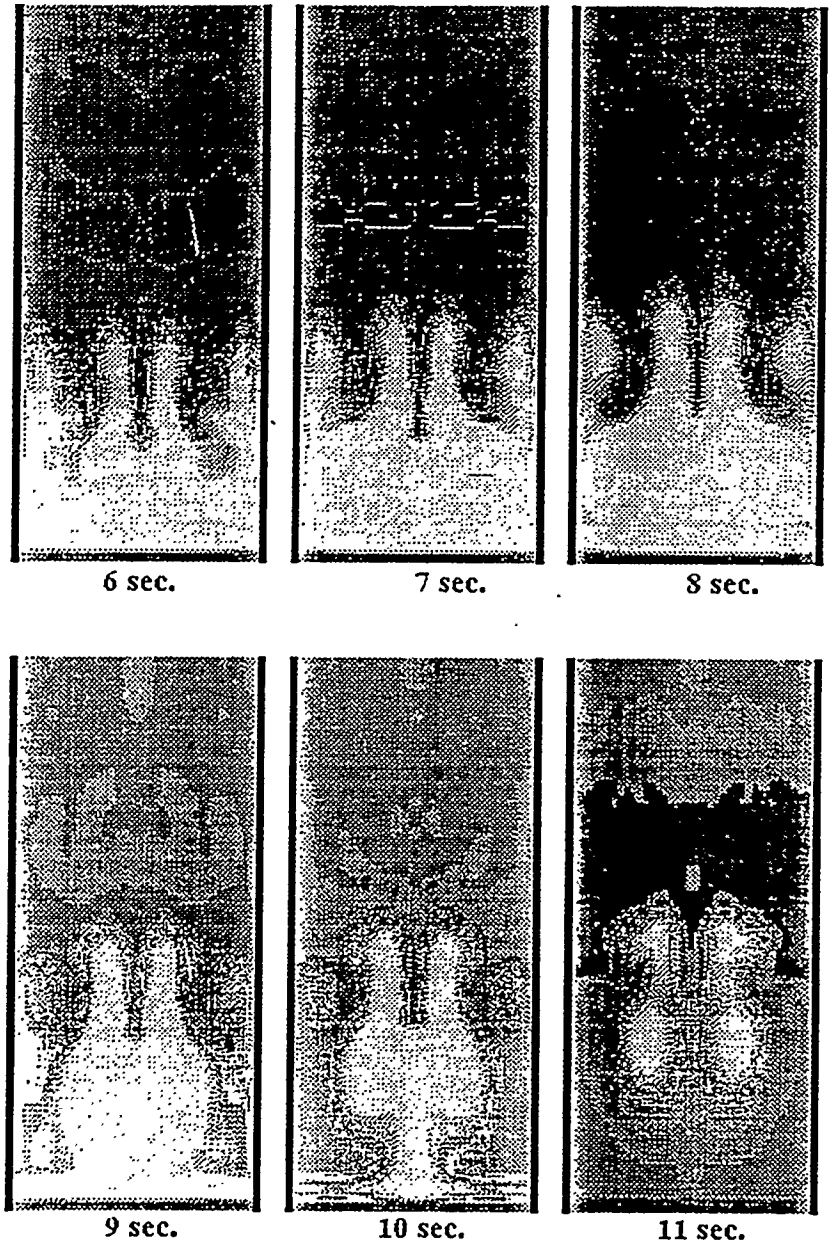

Figure 4.5b The Catalyst Concentration Profiles as a Function of Time

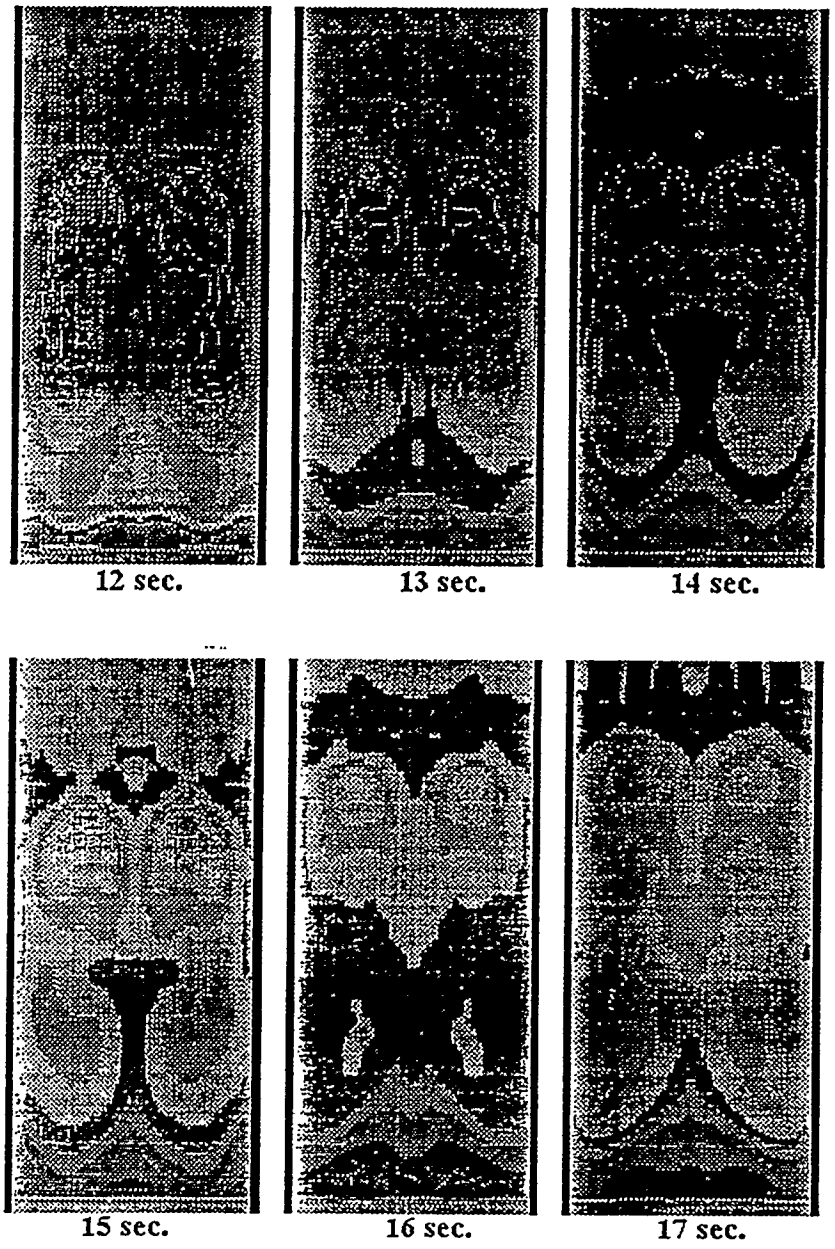

Figure 4.5c The Catalyst Concentration Profiles as a Function of Time

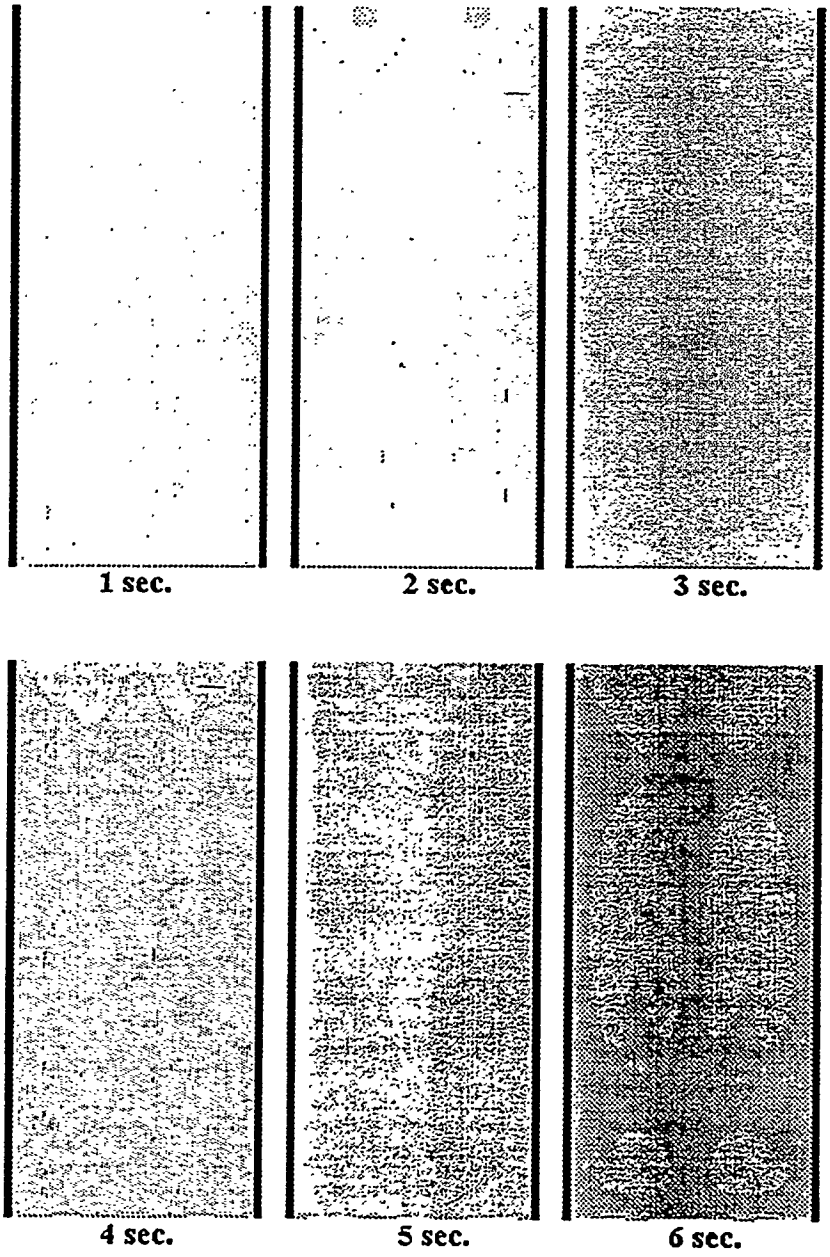

Figure 4.6a The Methanol Concentration Profiles as a Function of Time

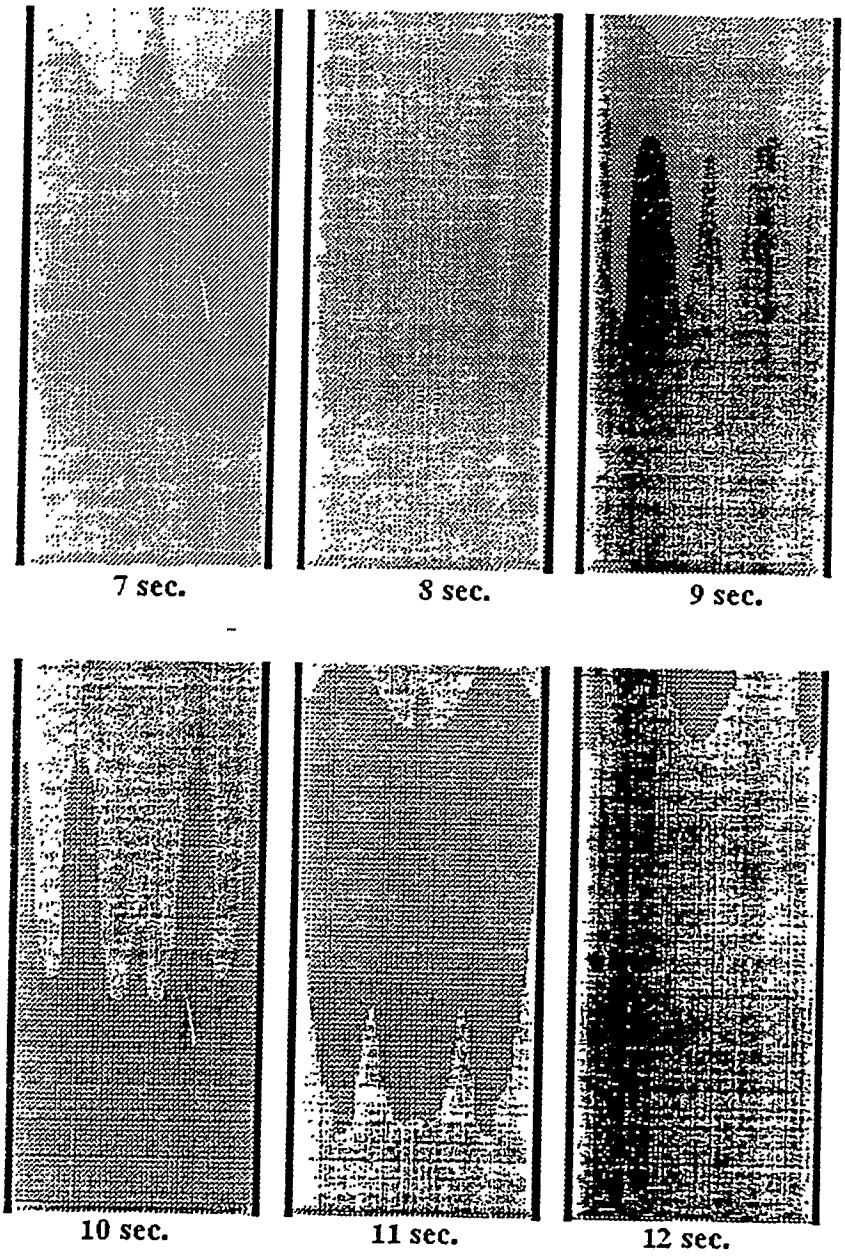

Figure 4.6b The Methanol Concentration Profiles as a Function of Time

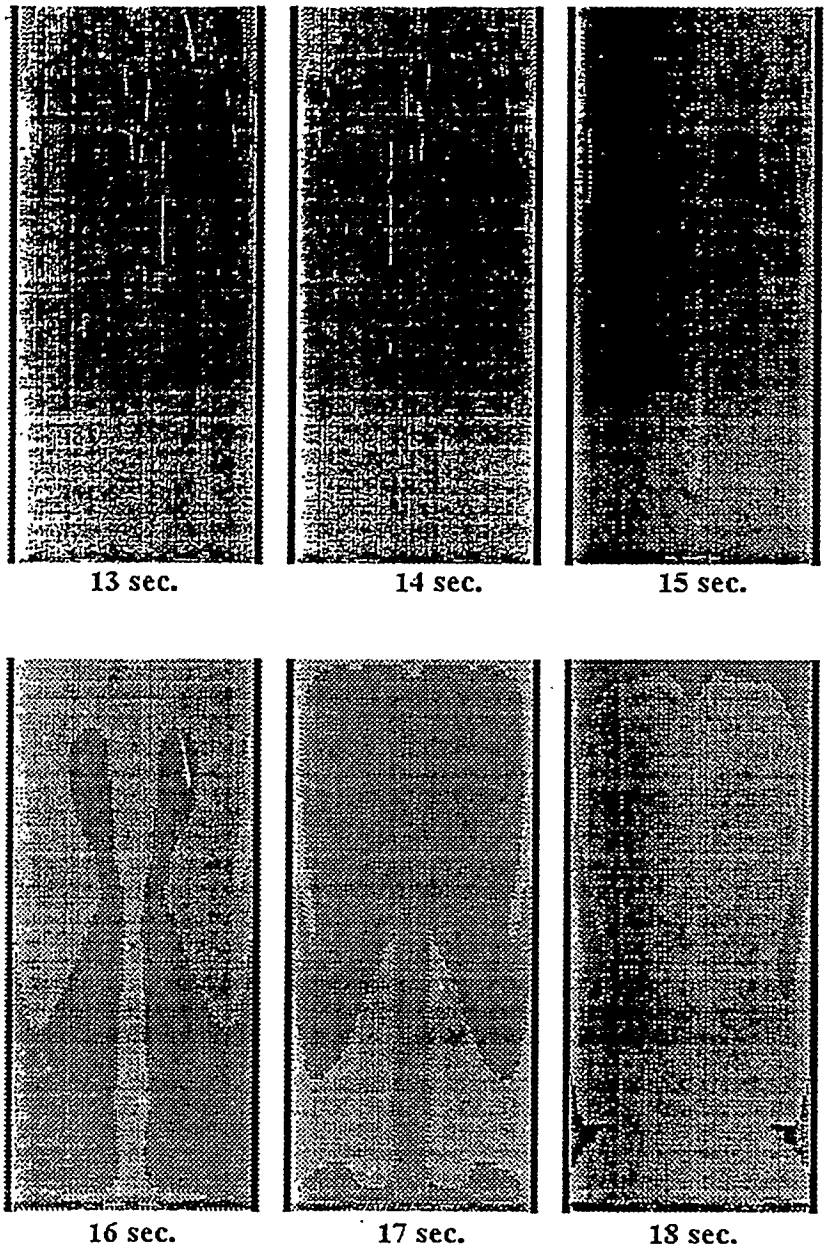

Figure 4.6c The Methanol Concentration Profiles as a Function of Time